Tissue Segmentation-Assisted Analysis of fMRI for Human Motor Response: An Approach Combining Artificial Neural Network and Fuzzy C Means

Ming-Jang Chiu, Chung-Chih Lin, Kai-Hsiang Chuang, Jyh-Horng Chen, and Kou-Mou Huang

The authors have developed an automated algorithm for segmentation of magnetic resonance images (MRI) of the human brain. They investigated the quantitative analysis of tissue-specific human motor response through an approach combining gradient echo functional MRI and automated segmentation analysis. Fifteen healthy volunteers, placed in a 1.5 T clinical MR imager, performed a self-paced finger opposition throughout the activation periods. T_1-weighted images (WI), T_2WI, and proton density WI were acquired for segmentation analysis. Single-slice axial T_2^* fast low-angle shot (FLASH) images were obtained during the functional study. Pixelwise cross-correlation analysis was performed to obtain an activation map. A cascaded algorithm, combining Kohonen feature maps and fuzzy C means, was applied for segmentation. After processing, masks for gray matter, white matter, small vessels, and large vessels were generated. Tissue-specific analysis showed a signal change rate of 4.53% in gray matter, 2.98% in white matter, 5.79% in small vessels, and 7.24% in large vessels. Different temporal patterns as well as different levels of activation were identified in the functional response from various types of tissue. High correlation exists between cortical gray matter and subcortical white matter (r = 0.957), while the vessel behaves somewhat different temporally. The cortical gray matter fits best to the assumed input function (r = 0.957) followed by subcortical white matter (r = 0.829) and vessels (r = 0.726). The automated algorithm of tissue-specific analysis thus can assist functional MRI studies with different modalities of response in different brain regions.

KEY WORDS: functional magnetic resonance imaging, human motor response, automated segmentation, Kohonen feature maps, fuzzy C means.

From the Departments of Neurology, Medical Informatics, and Radiology, College of Medicine, and the Institute of Electric Engineering, College of Electric Engineering, National Taiwan University, Taipei, Taiwan.

This study was supported by a grant from the National Science Council, Taiwan, NSC 88-2314-B-002-033-M08.

Address reprint requests to Jyh-Horng Chen, PhD, Institute of Electrical Engineering, College of Electrical Engineering, National Taiwan University, No 1, Sec 4, Roosevelt Rd, Taipei 105, Taiwan.

0897-1889/01/1401-0001$35.00/0
doi:10.1053/jdim.2001.21684

FUNCTIONAL magnetic resonance imaging (fMRI) is a powerful noninvasive tool for studying the physiology of functional activities in human brains. The underlying rationale for the endogenous contrast phenomenon is the blood oxygenation level dependent (BOLD) effect. Nevertheless, magnetic susceptibility-based fMRI is related to many complex changes, associated with neuronal activation such as regional blood volume and blood flow in addition to deoxyhemoglobin levels, that result in altered signal intensity in T_2^* or T_2-weighted MR images.[1-3] Therefore, a method capable of identifying the exact origin of the signal may become crucial. Does the functional response represent activation in the cerebral parenchyma or is it from interfering signals from extracerebral vasculature overlying the cerebral cortex?[4,5] Many studies have been designed and designated to delineate these controversies.[6-8]

Functional images usually are generated from conventional or echo planar imaging (EPI) gradient echo (GRE) studies. GRE fMRI is sensitive to decreased deoxyhemoglobin in activated brain tissue; however, it also is inherently vulnerable to the interference of inflow effect.[4-6] Thus, it induces large signal change at venous vessels during task activation.

In this report, we analyzed the motor response of the human brain through an approach combining GRE-based functional MRI and automated segmentation with MR images. We aimed to quantify the BOLD enhanced effect in the brain parenchyma and to separate it from inflow contribution from the extracerebral vessels. The addition of spatial anatomy helps to identify response signals with different temporal profiles and physiologic information from various sources.

MATERIALS AND METHODS

Fifteen healthy volunteers, with ages ranging from 24 to 52 years (30.5 ± 7.8 years), served as subjects in the study. The participants mainly were recruited from medical staff and medical and engineering students. All subjects gave their informed consent.

Experimental Procedure

We adopted the boxcar paradigm in the study. There were 3 alternating rest and activity periods for each subject. Subjects were asked to do finger opposition with their dominant hand in a fixed sequence. Subjects carried out the task repetitively and continuously at a self-paced rate of 1 to 2 Hz throughout the activation period. During the resting period, subjects laid down and relaxed without any motion. Sponges and straps were applied to enhance immobilization of the head throughout the experiment.

Image Acquisition

All images were acquired on a General Electric Signa 1.5 T clinical imager (Milwaukee, WI). In the experiment, 1 pair of temporomandibular-joint (TMJ) coils was placed symmetrically over both frontoparietal regions just above the motor cortex. Sagittal T_2-weighted images (T_2WI) with the fast spin echo pulse sequence were performed first as localizers for deciding the slice used in the functional study. These also were used as scout images to assure that both TMJ coils were positioned symmetrically and focused properly. On the midsagittal image, an axial slice through the middle of the precentral gyrus located between the cingulate sulcus and the cerebral vertex parallel to the bicommissural plane was chosen for the functional study. An axial T_1-weighted image (T_1WI) at the same level was acquired for the structure image. Axial T_2WI and proton density weighted images (PDWI) also were obtained for later segmentation analysis. The resolution of the T_1WI, T_2WI, and PDWI images is identical to that of the functional images described in the following. T_2^* fast low-angle shot (FLASH) pulse sequences, including typical parameters such as TR 110 ms/TE 50 ms/alpha = 40°/FOV 24 × 24/256 × 128/NEX = 1/slice thickness = 4 mm/flow compensated, were applied to generate the functional images. Each block consisted of 12 images, and the 3 pairs produced a total of 72 sequential images for one individual. All images were interpolated to form 256 × 256 matrix size.

Image Preprocessing by Automated Registration

To minimize the deteriorating effect from head movement, we applied image registration to reduce movement artifacts before further analysis. All functional images were aligned to the first image of each image series using the 2-dimensional rigid body model of AIR 3.0 (automated image registration) developed by R. P. Woods et al.[9] Sinc interpolation was used to minimize interpolation error.

Image Processing for Functional Response

Pixelwise cross-correlation (CC)[10,11] with a boxcar reference waveform, a square wave function (SWF), was applied to generate activation maps. In this study, the region of interest (ROI) was defined as a minimal rectangle encompassing the sensorymotor area contralateral to the activation side. To define the sensory motor area, we identified the central sulcus and superior frontal gyrus, and used the minimal rectangle to include the gyrus anterior and posterior to the sulcus (Fig 1). The rectangular region included parenchyma and cerebrospinal fluid (CSF) as well as the vascular space adjacent to the cerebral cortex. The average signal change in the ROI was calculated and expressed as a percentage, the mean signal change rate (mean SCR, Appendix 1). In ROI the pixels, whose signal intensity highly correlated temporally with the input SWF at the statistical level of $P < .01$, were considered activated. The number of pixels activated statistically was computed. To compare among subjects, the area of activation in the ROI was expressed as the relative activated area (RAA, Appendix 2), ie, the pixel number in the ROI of each subject was regarded as 100%.

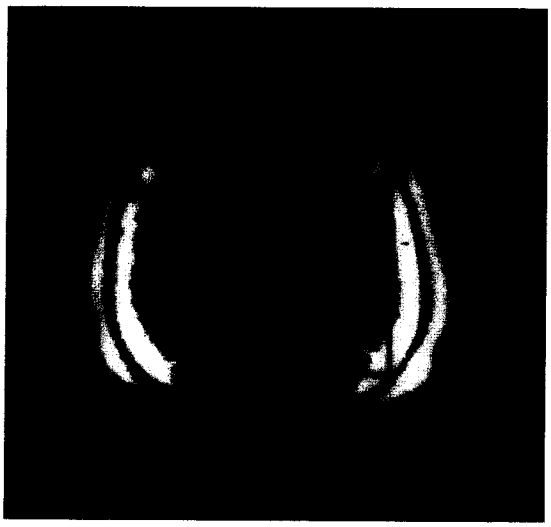

Fig 1. A T_1WI for the structure and the ROI.

Experimental Procedure

We adopted the boxcar paradigm in the study. There were 3 alternating rest and activity periods for each subject. Subjects were asked to do finger opposition with their dominant hand in a fixed sequence. Subjects carried out the task repetitively and continuously at a self-paced rate of 1 to 2 Hz throughout the activation period. During the resting period, subjects laid down and relaxed without any motion. Sponges and straps were applied to enhance immobilization of the head throughout the experiment.

Image Acquisition

All images were acquired on a General Electric Signa 1.5 T clinical imager (Milwaukee, WI). In the experiment, 1 pair of temporomandibular-joint (TMJ) coils was placed symmetrically over both frontoparietal regions just above the motor cortex. Sagittal T_2-weighted images (T_2WI) with the fast spin echo pulse sequence were performed first as localizers for deciding the slice used in the functional study. These also were used as scout images to assure that both TMJ coils were positioned symmetrically and focused properly. On the midsagittal image, an axial slice through the middle of the precentral gyrus located between the cingulate sulcus and the cerebral vertex parallel to the bicommissural plane was chosen for the functional study. An axial T_1-weighted image (T_1WI) at the same level was acquired for the structure image. Axial T_2WI and proton density weighted images (PDWI) also were obtained for later segmentation analysis. The resolution of the T_1WI, T_2WI, and PDWI images is identical to that of the functional images described in the following. T_2^* fast low-angle shot (FLASH) pulse sequences, including typical parameters such as TR 110 ms/TE 50 ms/alpha = 40°/FOV 24 × 24/256 × 128/NEX = 1/slice thickness = 4 mm/flow compensated, were applied to generate the functional images. Each block consisted of 12 images, and the 3 pairs produced a total of 72 sequential images for one individual. All images were interpolated to form 256 × 256 matrix size.

Image Preprocessing by Automated Registration

To minimize the deteriorating effect from head movement, we applied image registration to reduce movement artifacts before further analysis. All functional images were aligned to the first image of each image series using the 2-dimensional rigid body model of AIR 3.0 (automated image registration) developed by R. P. Woods et al.[9] Sinc interpolation was used to minimize interpolation error.

Image Processing for Functional Response

Pixelwise cross-correlation (CC)[10,11] with a boxcar reference waveform, a square wave function (SWF), was applied to generate activation maps. In this study, the region of interest (ROI) was defined as a minimal rectangle encompassing the sensorymotor area contralateral to the activation side. To define the sensory motor area, we identified the central sulcus and superior frontal gyrus, and used the minimal rectangle to include the gyrus anterior and posterior to the sulcus (Fig 1). The rectangular region included parenchyma and cerebrospinal fluid (CSF) as well as the vascular space adjacent to the cerebral cortex. The average signal change in the ROI was calculated and expressed as a percentage, the mean signal change rate (mean SCR, Appendix 1). In ROI the pixels, whose signal intensity highly correlated temporally with the input SWF at the statistical level of $P < .01$, were considered activated. The number of pixels activated statistically was computed. To compare among subjects, the area of activation in the ROI was expressed as the relative activated area (RAA, Appendix 2), ie, the pixel number in the ROI of each subject was regarded as 100%.

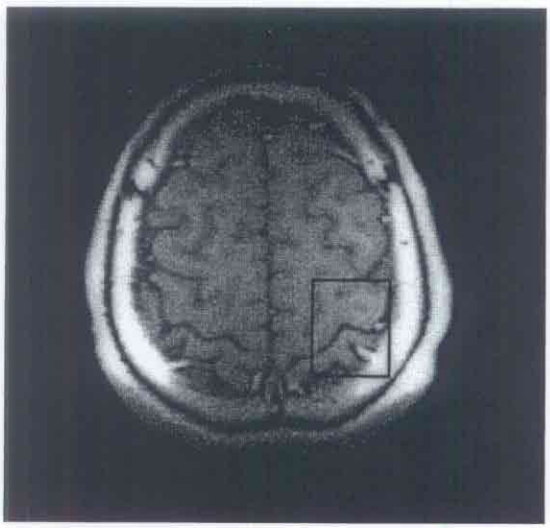

Fig 1. A T_1WI for the structure and the ROI.

Image Processing for Tissue Segmentation

The nonuniform properties of MRI make it rather difficult to decide a global threshold value effective for image segmentation using single contrast methods such as edge detection, threshold setting.[12,13] Hence, multispectral approaches are preferred for MRI segmentation in which multiple images for identification of textural features are necessary.[14,15] Algorithms for multispectral segmentation can be supervised or unsupervised. Because supervised methods are operator dependent, small differences in manually determined features might cause large interobserver or intraobserver variations in the results. Unsupervised methods are automated algorithms, which train themselves iteratively to get meaningful results. Therefore, unsupervised methods are clearly desirable in terms of reproducibility. The fuzzy C means (FCM) and a self-organizing feature map such as the Kohonen feature map (KFM), which were both applied in this study, are this type of method.

Therefore, we designed a cascaded algorithm combining the KFM (Appendix 3)[16] and FCM (Appendix 4)[17] in the image segmentation (Fig 2). There were 3 phases in this model. The first phase was an input layer used to receive data vectors from the source images. Input was from MR images with 3 different contrast weightings, ie, T_1WI, T_2WI, and PDWI spine-echo images. The second phase was to reduce the dimension of the source data ($3 \times 256 \times 256$) to a simple 8×8 feature map in which the optimal number of output neurons of the KFM was determined experimentally. The unsupervised 2-layered KFM was used to classify the pixels in brain images into categories. In the last phase, we labeled tissues in the source images. The output of the KFM was sent to the FCM to label tissues in the brain image. There were 6 clusters in the output layer of FCM, each representing the scalp, skull, meninges, gray matter, white matter, and CSF.

Finally, the segmented image became a mask for further analysis of the functional activation maps. An "AND" logical operation was then performed to combine activated pixels in ROI and the mask, which resulted in tissue specific activation.

One-way analysis of variance (ANOVA) with Scheffe's post hoc test was used to examine the significance of differences among tissue specific responses of the SCR and RAA. Correlation coefficients were computed pairwise between temporal profiles of different tissues.

RESULTS

In spite of instruction and a device immobilizing the subject's head during the experiment, we had to exclude one subject whose motion artifact was so severe that we could not overcome it even after image registration. The activation map was generated by overlaying a T_1-weighted image with activated pixels at the significance level of $P < .01$ obtained from a pixelwise CC processing (Fig 3). The statistical threshold of the activation map was decided rather arbitrarily. With a higher threshold,

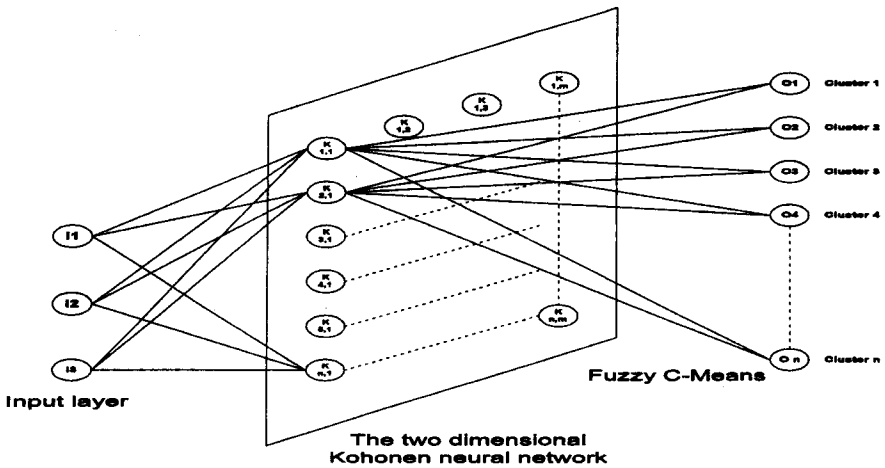

Fig 2. Structure of the cascaded algorithm combining the Kohonen neural network and fuzzy C-means.

Fig 3. A functional activation map generated from pixel-wise cross correlation analysis at the significance level of $P < .01$ superimposed on a T_1-weighted image.

eg, $P < .001$, we obtained less noise and a higher mean SCR, but, at the same time, fewer activated pixels and a smaller RAA. In contrast, a lower threshold, eg, $P < .05$, incurred many probably irrelevant activated pixels and a lower mean SCR. The significance level of $P < .01$ was chosen on an empirical ground after considering all these tradeoffs. The mean SCR ($P < .01$) in the ROI of 14 subjects was 5.60 ± 1.84% and ranged from 3.19% to 10.12%, whereas the mean RAA was 17.00 ± 6.16 (Table 1).

Image processing for tissue segmentation classified pixels of the MR image into 6 clusters. Usually, the outer rim of the image, including the skull, scalp, or edge artifacts from motion was segregated as 1 or as several clusters separate from other components of the inner structures (Fig 4). In most cases, the pia matter and annexed small cortical vessels (small vessels) were classified into 1 individual cluster, keeping the overlying large cerebral vessels (large vessels) and surrounding CSF space apart. The cortical gray matter and subcortical white matter were separated into different clusters. However, in some cases it was necessary to combine 2 clusters to fulfill the picture of either cortical gray matter (Fig 5A) or subcortical white matter (Fig 6A). To have a comprehensive understanding of the signal contribution of the inflow effect, we combined clusters from small and large vessels (Fig 7A).

Table 1. Functional Response in the Region of Interest and Tissue-Specific Areas

	Mean (n = 14)	SD	Ratio (1/White matter)
Region of interest			
RAA (%)	17.00	6.16	13.30
Mean SCR (%)	5.60	1.84	1.88
Gray matter (G)			
RAA (%)	7.33	3.64	5.73
Mean SCR (%)	4.53	1.38	1.52
White matter (W)			
RAA (%)	1.28	1.09	1.00
Mean SCR (%)	2.98	1.31	1.00
Parenchyma (G + W)			
RAA (%)	8.60	3.95	6.73
Mean SCR (%)	4.39	1.33	1.47
Small vessels			
RAA (%)	4.36	2.38	3.42
Mean SCR (%)	5.79	1.88	1.94
Large vessels			
RAA (%)	3.72	2.05	2.91
Mean SCR (%)	7.24	2.41	2.43
Vessels (small + large)			
RAA (%)	8.09	3.38	6.33
Mean SCR (%)	6.54	2.02	2.20

An "AND" logical operation between the activated pixels and the mask resulted in the tissue-specific functional response (Figs 5B, 6B, 7B). The 1-way ANOVA test on 4 tissue categories, including cortical gray matter, subcortical white matter, small vessels, and large vessels, showed significant

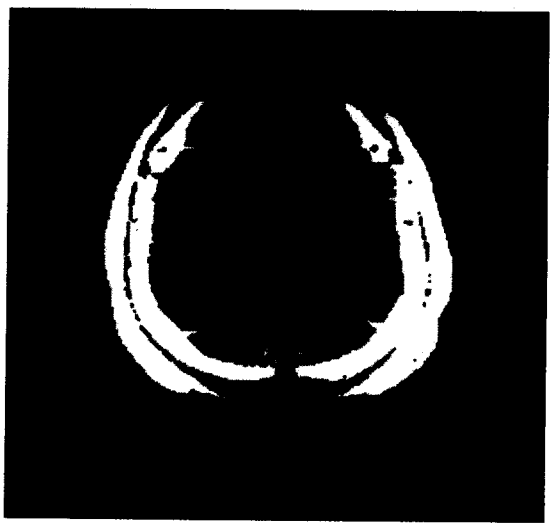

Fig 4. Outer rim of the magnetic resonance image obtained from the Kohonen feature map/fuzzy C-means algorithm.

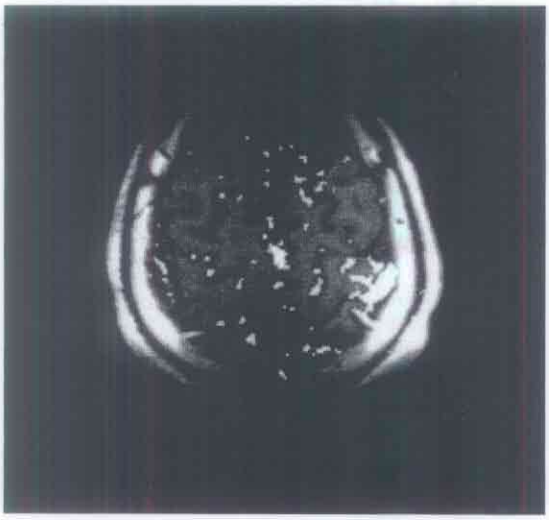

Fig 3. A functional activation map generated from pixel-wise cross correlation analysis at the significance level of $P < .01$ superimposed on a T_1-weighted image.

eg, $P < .001$, we obtained less noise and a higher mean SCR, but, at the same time, fewer activated pixels and a smaller RAA. In contrast, a lower threshold, eg, $P < .05$, incurred many probably irrelevant activated pixels and a lower mean SCR. The significance level of $P < .01$ was chosen on an empirical ground after considering all these tradeoffs. The mean SCR ($P < .01$) in the ROI of 14 subjects was 5.60 ± 1.84% and ranged from 3.19% to 10.12%, whereas the mean RAA was 17.00 ± 6.16 (Table 1).

Image processing for tissue segmentation classified pixels of the MR image into 6 clusters. Usually, the outer rim of the image, including the skull, scalp, or edge artifacts from motion was segregated as 1 or as several clusters separate from other components of the inner structures (Fig 4). In most cases, the pia matter and annexed small cortical vessels (small vessels) were classified into 1 individual cluster, keeping the overlying large cerebral vessels (large vessels) and surrounding CSF space apart. The cortical gray matter and subcortical white matter were separated into different clusters. However, in some cases it was necessary to combine 2 clusters to fulfill the picture of either cortical gray matter (Fig 5A) or subcortical white matter (Fig 6A). To have a comprehensive understanding of the signal contribution of the inflow effect, we combined clusters from small and large vessels (Fig 7A).

Table 1. Functional Response in the Region of Interest and Tissue-Specific Areas

	Mean (n = 14)	SD	Ratio (1/White matter)
Region of interest			
RAA (%)	17.00	6.16	13.30
Mean SCR (%)	5.60	1.84	1.88
Gray matter (G)			
RAA (%)	7.33	3.64	5.73
Mean SCR (%)	4.53	1.38	1.52
White matter (W)			
RAA (%)	1.28	1.09	1.00
Mean SCR (%)	2.98	1.31	1.00
Parenchyma (G + W)			
RAA (%)	8.60	3.95	6.73
Mean SCR (%)	4.39	1.33	1.47
Small vessels			
RAA (%)	4.36	2.38	3.42
Mean SCR (%)	5.79	1.88	1.94
Large vessels			
RAA (%)	3.72	2.05	2.91
Mean SCR (%)	7.24	2.41	2.43
Vessels (small + large)			
RAA (%)	8.09	3.38	6.33
Mean SCR (%)	6.54	2.02	2.20

An "AND" logical operation between the activated pixels and the mask resulted in the tissue-specific functional response (Figs 5B, 6B, 7B). The 1-way ANOVA test on 4 tissue categories, including cortical gray matter, subcortical white matter, small vessels, and large vessels, showed significant

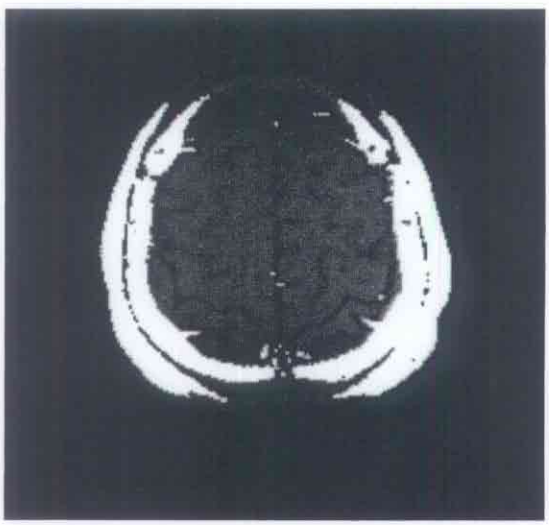

Fig 4. Outer rim of the magnetic resonance image obtained from the Kohonen feature map/fuzzy C-means algorithm.

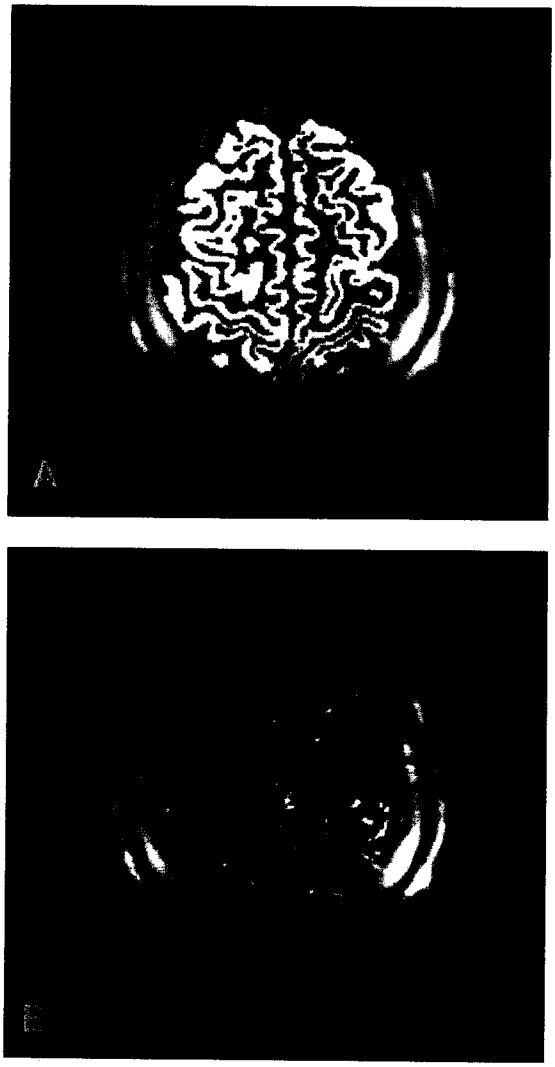

Fig 5. (A) Mask for cortical gray matter. (B) Functional activation map of cortical gray matter.

differences in terms of the RAA ($F = 14.22$; $P < .0001$) and mean SCR ($F = 14.21$; $P < .0001$). Analysis on the tissue specific mean RAA showed that most functional response occurred in the cortical gray matter (7.33 ± 3.64; Scheffe's post hoc test, $P < .05$; Table 2). The second most functional response was in small vessels in the pia matter (RAA = 4.36 ± 2.38), and the third was in the large vessels in the CSF space (RAA = 3.72 ± 2.05). The subcortical white matter had very few responses (RAA = 1.28 ± 1.09). Analysis of the mean SCR showed significantly higher rates of response in the large vessels than in the parenchyma, both in cortical gray and subcortical white matter (Scheffe's post hoc test, $P < .05$; Table 2). However, there was no significant difference between small and large vessels in terms of the RAA or mean SCR (Scheffe's post hoc test; $P > .05$; Table 2). Therefore, the inflow effect is represented reasonably by the sum-up response (mean SCR = 6.54 ± 2.02%) from both small and large vessels.

Finally, various temporal profiles in accordance with tissue specificity were identified. The time course was calculated by averaging tissue specific mean signal intensity in the ROIs of all 14 subjects at each time-point. The sequential 72 images acquired thus were considered as 72 continuous time-

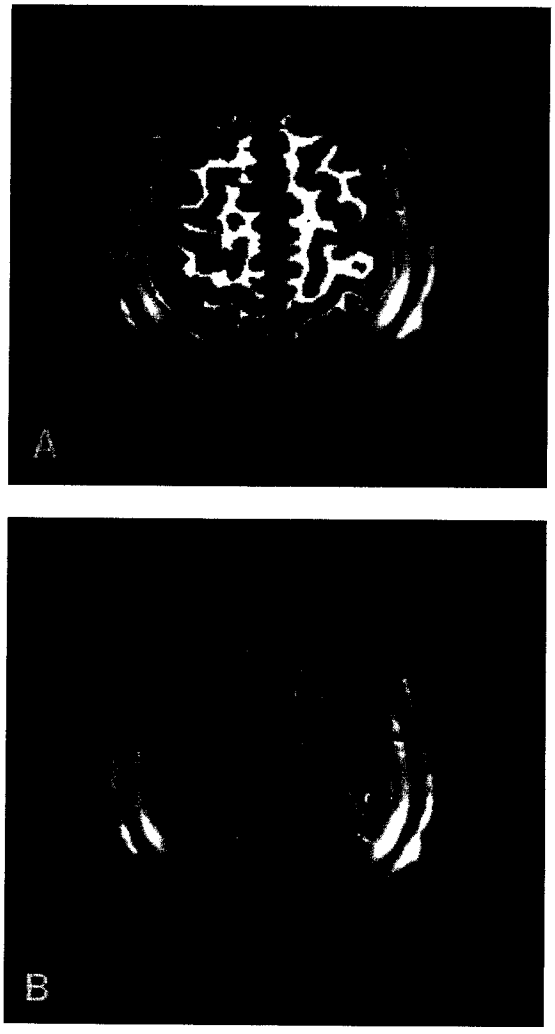

Fig 6. (A) Mask for white matter. (B) Functional activation map of white matter.

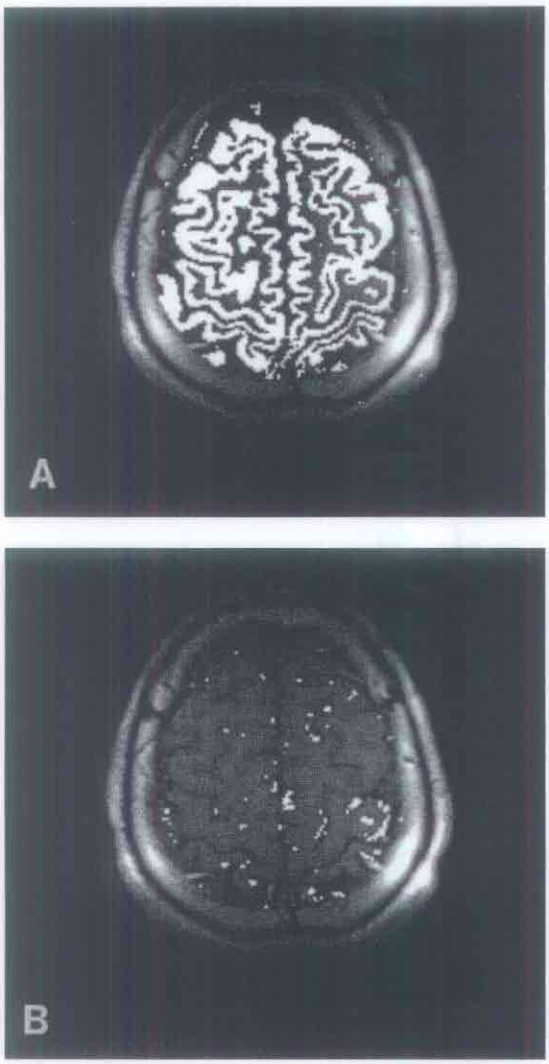

Fig 5. (A) Mask for cortical gray matter. (B) Functional activation map of cortical gray matter.

differences in terms of the RAA ($F = 14.22$; $P < .0001$) and mean SCR ($F = 14.21$; $P < .0001$). Analysis on the tissue specific mean RAA showed that most functional response occurred in the cortical gray matter (7.33 ± 3.64; Scheffe's post hoc test, $P < .05$; Table 2). The second most functional response was in small vessels in the pia matter (RAA = 4.36 ± 2.38), and the third was in the large vessels in the CSF space (RAA = 3.72 ± 2.05). The subcortical white matter had very few responses (RAA = 1.28 ± 1.09). Analysis of the mean SCR showed significantly higher rates of response in the large vessels than in the parenchyma, both in cortical gray and subcortical white matter (Scheffe's post hoc test, $P < .05$; Table 2). However, there was no significant difference between small and large vessels in terms of the RAA or mean SCR (Scheffe's post hoc test; $P > .05$; Table 2). Therefore, the inflow effect is represented reasonably by the sum-up response (mean SCR = $6.54 \pm 2.02\%$) from both small and large vessels.

Finally, various temporal profiles in accordance with tissue specificity were identified. The time course was calculated by averaging tissue specific mean signal intensity in the ROIs of all 14 subjects at each time-point. The sequential 72 images acquired thus were considered as 72 continuous time-

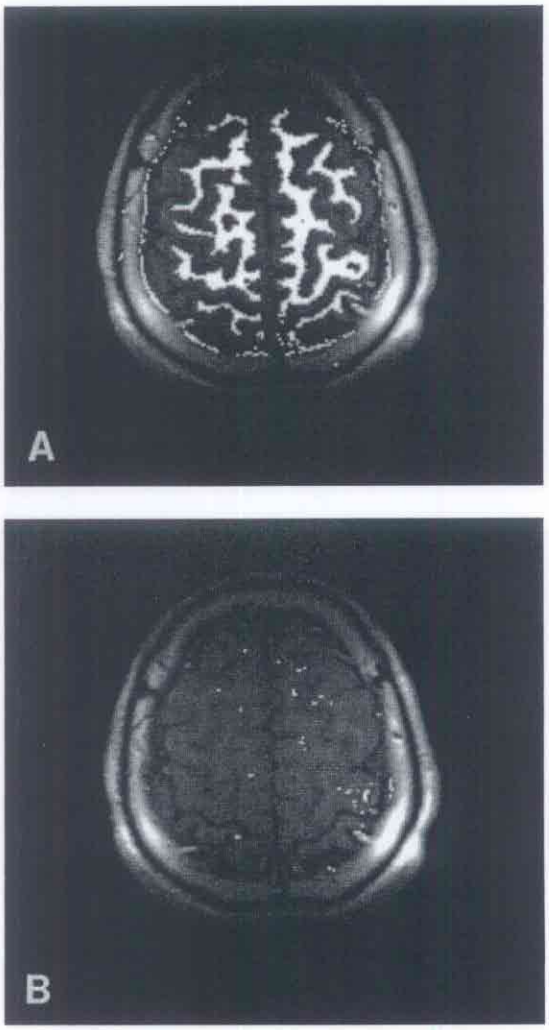

Fig 6. (A) Mask for white matter. (B) Functional activation map of white matter.

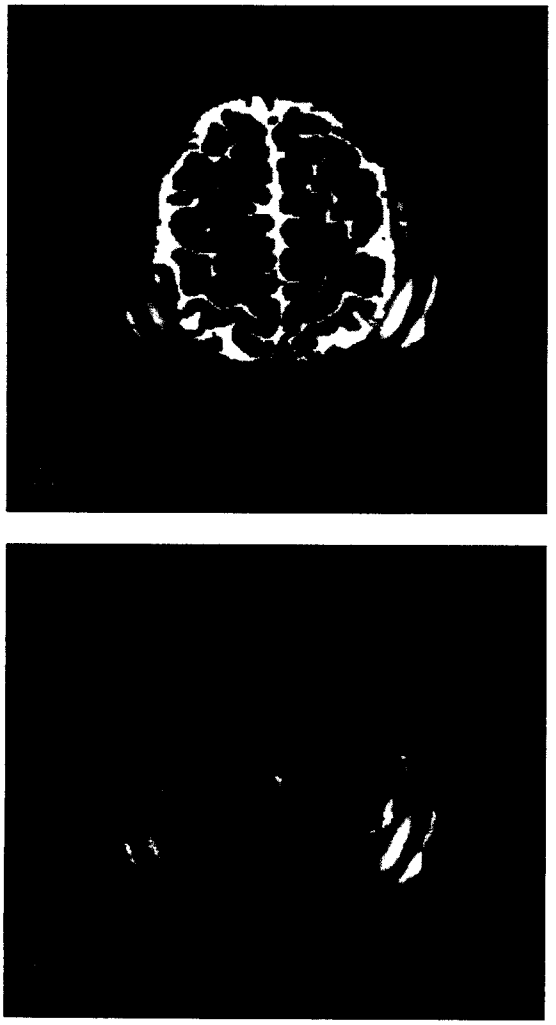

Fig 7. (A) Mask for the CSF space. (B) Functional activation map from vessels in the meninges and CSF space.

points. The correlation between 2 compartments of the vessel space, which consisted of the small vessels overlying the cortex and the large vessels in the CSF, is rather high (r = 0.976), and it is again reasonable that we considered it as a single entity for further analysis and discussion. The correlation study also showed a very high correlation coefficient between temporal patterns of cortical gray matter and subcortical white matter (r = 0.957). The correlation was somewhat lower between cortical gray matter and vessels (r = 0.723) as well as between subcortical white matter and vessels (r = 0.713). There also were different levels of correlation in terms of the assumed input fuction, the SWF of a boxcar paradigm. The correlation coefficient between the SWF and the cortical gray matter was r = 0.957, and between the SWF and the subcortical white matter it was r = 0.829, and between the SWF and the vessells it was r = 0.726. The sustained responses from either cortical gray matter or subcortical white matter contrasted themselves from the initially declining time course of response in the vessel space (Fig 8). The diagram showed at the same time that the response from the vessels had intrinsically higher signal intensity than the parenchyma along the time course after baseline correction.

DISCUSSION

To overcome the low signal-to-noise ratio (SNR) obtained from the standard head coil in our system, we used surface TMJ coils. Because surface coils may introduce variations from coil position and spatial nonuniformity of signal, we had to be cautious in placing the coils and sometimes had to readjust them under the guidance of scout images. However, the SNR is very important in an fMRI study and this caution is necessary. In addition, the target we investigated ie, the motor cortex, which is relatively superficial in anatomical position, is within the effective range of surface coils. Therefore, the problem of the inhomogenity was not detrimental to the results of this study.

Because FCM provides an iterative approach to

Table 2. Result of Scheffe's Post Hoc Test in Tissue-Specific Areas ($P < .05$)

	Gray Matter		White Matter		Small Vessels		Large Vessels	
	RAA	MSCR	RAA	MSCR	RAA	MSCR	RAA	MSCR
Gray matter	–	–						
White matter	*	NS	–	–				
Small vessels	*	NS	*	*	–	–		
Large vessels	*	*	NS	*	NS	NS	–	–

Abbreviations: NS, no significance; MSCR, mean signal change rate.
* Positive with Scheffe's post hoc test, $P < .05$.

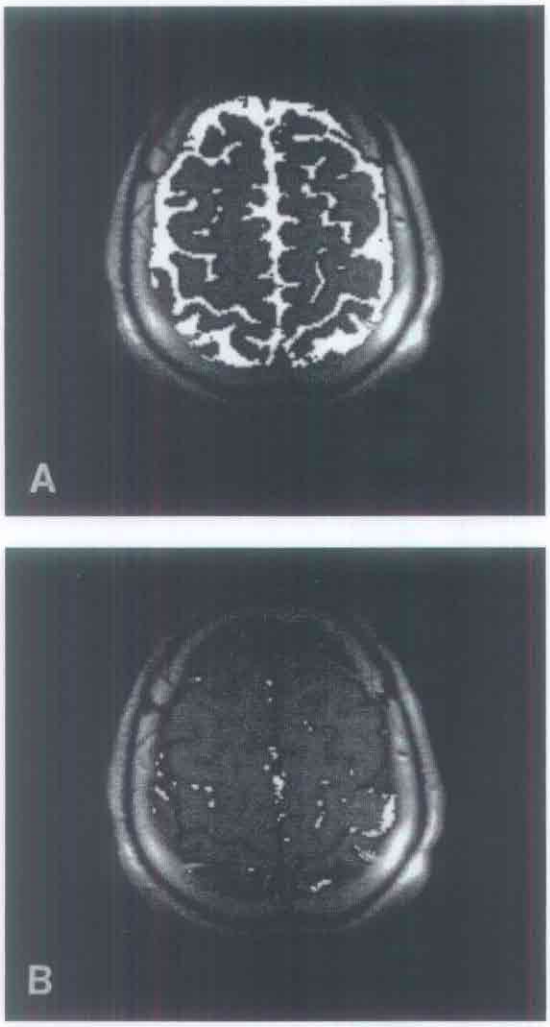

Fig 7. (A) Mask for the CSF space. (B) Functional activation map from vessels in the meninges and CSF space.

points. The correlation between 2 compartments of the vessel space, which consisted of the small vessels overlying the cortex and the large vessels in the CSF, is rather high (r = 0.976), and it is again reasonable that we considered it as a single entity for further analysis and discussion. The correlation study also showed a very high correlation coefficient between temporal patterns of cortical gray matter and subcortical white matter (r = 0.957). The correlation was somewhat lower between cortical gray matter and vessels (r = 0.723) as well as between subcortical white matter and vessels (r = 0.713). There also were different levels of correlation in terms of the assumed input fuction, the SWF of a boxcar paradigm. The correlation coefficient between the SWF and the cortical gray matter was r = 0.957, and between the SWF and the subcortical white matter it was r = 0.829, and between the SWF and the vessells it was r = 0.726. The sustained responses from either cortical gray matter or subcortical white matter contrasted themselves from the initially declining time course of response in the vessel space (Fig 8). The diagram showed at the same time that the response from the vessels had intrinsically higher signal intensity than the parenchyma along the time course after baseline correction.

DISCUSSION

To overcome the low signal-to-noise ratio (SNR) obtained from the standard head coil in our system, we used surface TMJ coils. Because surface coils may introduce variations from coil position and spatial nonuniformity of signal, we had to be cautious in placing the coils and sometimes had to readjust them under the guidance of scout images. However, the SNR is very important in an fMRI study and this caution is necessary. In addition, the target we investigated ie, the motor cortex, which is relatively superficial in anatomical position, is within the effective range of surface coils. Therefore, the problem of the inhomogenity was not detrimental to the results of this study.

Because FCM provides an iterative approach to

Table 2. Result of Scheffe's Post Hoc Test in Tissue-Specific Areas ($P < .05$)

	Gray Matter		White Matter		Small Vessels		Large Vessels	
	RAA	MSCR	RAA	MSCR	RAA	MSCR	RAA	MSCR
Gray matter	—	—						
White matter	*	NS	—	—				
Small vessels	*	NS	*	*	—	—		
Large vessels	*	*	NS	*	NS	NS	—	—

Abbreviations: NS, no significance; MSCR, mean signal change rate.
* Positive with Scheffe's post hoc test, $P < .05$.

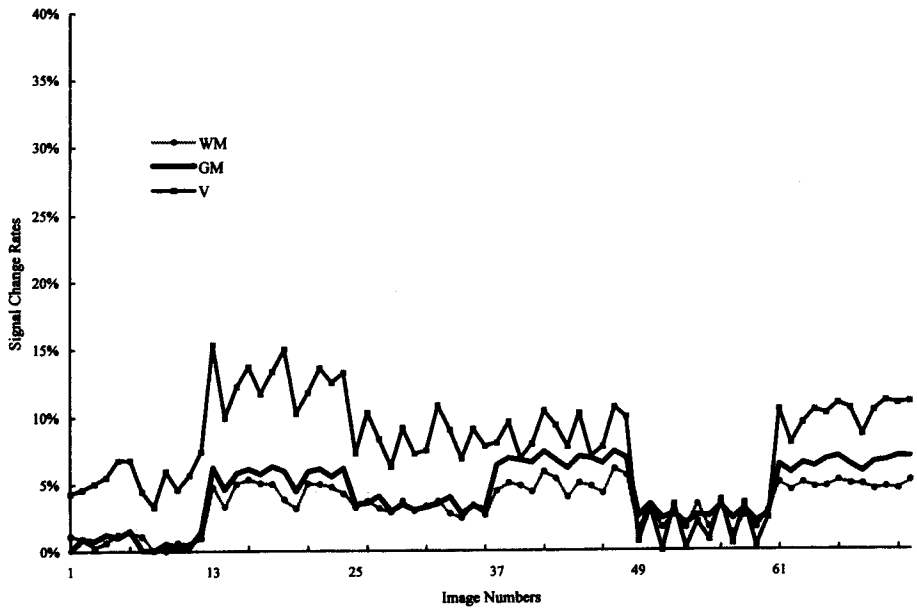

Fig 8. The chart shows 3 different temporal patterns with different activation levels from different brain tissues for human motor response. WM, white matter; GM, gray matter; and V, vessel space. The Y-axis indicates the signal change rates and the X-axis indicates the sequential image numbers considered as continuous time points.

approximate the minimum of the objective function starting from a given position, it usually is applicable to tissue classification. However, FCM often requires long computation time because of the complexity of the algorithm.[18] However, the KFM distributes original data on a 2-dimensional map, in our case an 8 · 8 matrix, in which similar input signal patterns are joined together with adjacent nodes on a map.[16] The KFM has excellent computational performance, but it is influenced easily by factors such as initial condition, learning rate, and update rule, which may then generate variable results (unpublished data). This is why we applied such a complex cascaded architecture instead of either single method alone. Using this architecture, we benefit from the efficiency of the KFM in terms of high computation power and low memory load for the computer as well as the optimization capability of FCM.[19]

Furthermore, the performance of either the KFM or FCM is decided by the internal parameters of the systems. There always is a tradeoff between effectiveness and efficiency in deciding of various internal parameters. For example, increasing the cluster number of either the KFM or FCM could elevate specificity and make the pattern of the smaller area size easier to identify.[20] However, too many clusters will overclassify the patterns, thus making the results very difficult to analyze and interpret. In addition, a large cluster number increases the processing time. For further details about the performance, internal parameters and validation of the algorithms readers are referred to our previous work.[19-21]

In this study, the T_1, T_2, and PD are parameters capable of tissue characterization.[21-23] Using these parameters, we showed that the process of automated image segmentation, which cascades the KFM and FCM algorithms, can effectively separate anatomic structures in MR images (Figs 4, 5A, 6A, 7A). This makes possible the tissue-specific analysis of functional activation in the brain.

However, the issue of partial volume effect (PVE) must be considered here, because it might indicate some limitation on our algorithm with present hardware settings. We used a resolution of 256 × 256 (interpolated from images with a resolution of 256 × 128) on an FOV of 24 × 24 cm with our MR images, either with morphologic or functional images. Therefore, the voxel is around $1 \times 1 \times 4$ mm^3, which probably makes the segmentation susceptible to the PVE especially in the direction of thickness. Thus, there are always some pixels, at the border of the gray matter and white

matter, containing tissues from either side. Nevertheless, the scale of the problem may not be so large as to significantly influence the results of the segmentation or tissue-specific analysis of our functional response. After all, the mixing of tissues caused by the PVE may occur only in pixels at the border of the 2 tissues. The number or proportion of these pixels is quite limited. The problem of PVE in tissue segmentation can be alleviated but not resolved by recent advances in hardware settings, eg, higher image resolution with higher Tesla machines. However, even with echo planar fMRI, which is used frequently nowadays, many researchers prefer to perform their functional studies with even lower resolution, eg, 64 × 64, because the signal intensity and time resolution is of more the concern in many studies.

The FLASH sequence is important in terms of functional MRI studies. Nonetheless, FLASH is inherently sensitive to the inflow effect, which is especially high when we apply a large flip angle and long TE.[7,8] The inflow effect may be undesirable because the BOLD effect is the only focus of interest in many fMRI experiments. In this study, we separated activation into the BOLD effect, which is confined to the parenchyma and mainly over the cortical gray matter, and the inflow effect, which is mainly derived from the overlying cortical vasculature. Therefore, additional spatial information offers the magnitude of influence and a temporal pattern of response in the blood vessel. In this study, we applied a pulse sequence with a large flip angle ($\alpha = 40°$) and a long TE (TE = 50 ms) with flow compensation to accentuate the inflow effect. With the help of this new technique, we can separate the response of vessels such as cortical veins or meningeal arterioles from the BOLD effect in the cerebral parenchyma. However, the flow sensitivity of FLASH images applies only to those vessels with proper orientation and flow velocity in our single slice method. Thus, we do not claim to replace other flow-sensitive techniques such as flow-sensitive alternating inversion recovery (FAIR).[6,24] Nevertheless, we do isolate the response and activity in the parenchyma and reduce the influence of inflow effect to a substantial degree. Furthermore, the tissue-specific response provides the delineation of temporal profiles from different physiologic sources (Fig 8). High correlation exists between cortical gray matter and subcortical white matter (r = 0.957), which implies a similarity of response in the parenchyma from gray and white matter. However, the vessel behaves somewhat different temporally in response to the neural activation. We computed the functional response by cross correlation between an assumed square wave input function of the boxcar paradigm and the signal intensity changes on MR images. Although the genuine tissue-specific process (response curve) in the brain is not known, our results showed that the cortical gray matter fits best to the assumed SWF (r = 0.957) followed by subcortical white matter (r = 0.829) and vessels (r = 0.726). The phenomenon is worth exploring further especially the different modalities of brain activation such as somatosensory, visual, or high cortical functions. Further comparison with results from other data-driven analysis[21,25] also should be considered.

We analyzed the motor response of the human brain through an approach combining the pulse sequence of functional MRI, the accentuating inflow effect, and a cascade algorithm performing effective automated image tissue segmentation. This approach enables tissue-specific analysis and separates activation with different temporal patterns in human motor responses. It reduces the disadvantage of inflow vulnerability in conventional GE and provides quantification and separation of BOLD enhancement effects from inflow contributions in an activated human brain. Tissue segmentation provides the most natural basis for neuroscientists, who are already acquainted with the anatomy of the human brain, to do data analysis. This technique may become a new helpful tool for GRE fMRI.

APPENDIX 1

The mean SCR is obtained from the following equation:

$$SCR_P = \left(\frac{\frac{1}{N_A}\sum_{i=1}^{N_A} S_{Ai} - \frac{1}{N_R}\sum_{i=1}^{N_R} S_{Ri}}{\frac{1}{N_R}\sum_{i=1}^{N_R} S_{Ri}} \right) \times 100\%$$

$$meanSCR = \frac{1}{N_P}\sum_{P=1}^{N_P} SCR_P$$

Where S_A is the signal intensity of pixel P during the activating period; S_R is the counterpart of S_A during the resting period; N_A is the number of the time-series images in the activating period; N_R is

the number in the resting period; in our study $N_A = N_R$; SCR_P is the signal change rate of an activated pixel expressed as a percentage; N_P is the number of all the activated pixels, obtained by a threshold procedure with the cross correlation, in the ROI.

APPENDIX 2

The relative activated area is computed from the following equation:

$$RAA = \frac{N_P}{N_{ROI}} \times 100\%$$

Where N_P is the number of all activated pixels selected by a threshold procedure ($P < .01$) with CC confined in the ROI; N_{ROI} is the number of all pixels contained in the ROI.

APPENDIX 3

The KFM is a model of a self-organized feature map, which is capable of clustering the inner structures or intrinsic characteristics of a data set automatically. The core idea of this network is "winner-take-all." It has a 2-layer structure. The first layer, the input layer, receives the variables of the whole network. The second layer is the competitive layer or so-called output layer. It expresses the output as classification of the training set. The learning algorithm of the Kohonen feature map is as follows:

$$\Delta W_{ij} = \eta \times (X_i - W_{ij}) \times R$$

Where η is the learning rate of the network, R is the radius of convergence, and D is the distance between the winner and other output nodes. When all of the output nodes are updated according to the learning algorithm, the average error is calculated as the criteria of the convergence of the system. The average error is calculated as follows:

$$D_m = \sum_{i}^{Pixel} \sum_{i}^{Vector} |X_{i,j} - W_{winner,j}|$$

Where X_{ij} is the jth vector of the ith input unit; $W_{winner,j}$ is the weighting vector of the winner node in the output layer. This algorithm will iterate until $\frac{|D_m - D_{m+1}|}{D_m} < \epsilon$, ϵ is the criterion of convergence, which was 10^{-4} in this study.

When the amount of modification is below a certain threshold, the system training is finished. Then all the weighting values in the network were saved for further classification.

APPENDIX 4

The basic idea of the fuzzy theorem is that it attributes to each event of interest a fuzzy set of membership functions with a probability of occurrence. Instead of simply classifying every input into a definite cluster, the final decision is made according to a membership function of each event. The membership function is the probability for a pixel to be attributed to a certain cluster in the image segmentation. A distant feature implies a smaller probability of the attribution. The value of a membership function lies between 0 and 1. The sum of all clusters is 1. For convenience, we expressed the probability of each pixel with a c × n matrix U, which was called the fuzzy C partition or membership matrix. C is the total cluster number and n is the total pixel number. Then we iterate with the principle of least-squares error to locate the optimal center of the clusters. The purpose of the optimization was to minimize the objective function:

$$J_m(U, V) = \sum_{k=1}^{n} \sum_{i=1}^{c} (U_{ik})^m \|X_k - V_i\|^2,$$

Where U_{ik} represents the membership function of the k^{th} pixel belonging to the i^{th} cluster; X_k is the feature vector of the k^{th} pixel; V_i is the center feature vector of the i^{th} cluster; m is an adjustable parameter usually ranging between 1.1 and 5.0.

REFERENCES

1. Ogawa S, Lee TM, Kay AR, et al: Brain magnetic resonance imaging with contrast dependent on blood oxygenation. Proc Natl Acad Sci U S A 87:9868-9872, 1992

2. Ogawa S, Lee TM, Nayak AS, et al: Oxygen-sensitive contrast in magnetic resonance image of rodent brain at high magnetic fields. Magn Reson Med 14:68-78, 1990

3. Kwong KK, Belliveau JW, Chesler DA, et al: Dynamic magnetic imaging of human brain activity during primary sensory stimulation. Proc Natl Acad Sci U S A 89:5675-5679, 1992

4. Duyn JH, Moonen CTW, van Yperen GH, et al: Inflow versus deoxyhemoglobin effects in BOLD functional MRI using gradient echoes at 1.5 T. NMR Biomed 7:83-88, 1994

5. Segbearth C, Belle V, Delon C, et al: Functional MRI of the human brain: Predominance of signals from extracerebral veins. Neuroreport 5:831-836, 1994

6. Kim SG, Ugurbil K: Comparison of blood oxygenation and cerebral blood flow effects in fMRI: Estimation of relative oxygen consumption change. Magn Reson Med 38:59-65, 1997

7. Gao JH, Miller I, Lai S, et al: Quantitative assessment of blood inflow effects in functional MRI signals. Magn Reson Med 36:314-319, 1996

8. Gati JS, Menon RS, Ugurbil K, et al: Experimental determination of the BOLD field strength dependence in vessels and tissue. Magn Reson Med 38:296-302, 1996

9. Woods RP, Cherry SR, Mazziotta JC: Rapid automated algorithm for aligning and reslicing PET images. J Comput Assist Tomogr 16:620-633, 1992

10. Bandettini PA, Wong EC, Hinks RS, et al: Time course EPI of human brain function during task activation. Magn Reson Med 25:390-397, 1992

11. Bandettini PA, Jesmanovicz A, Wong EC, et al: Processing strategies for time-course data sets in functional MRI of the human brain. Magn Reson Med 30:161-173, 1993

12. Clarke LP, Velthuizen RP, Camacho MA, et al: MRI segmentation: Methods and applications. Magn Reson Imaging 13:343-368, 1995

13. Bomans M, Hohne KH, Tiede U, et al: 3D segmentation of MR images of the head for 3-D display. IEEE Trans Med Imaging 9:177-183, 1990

14. Bezdek JC, Hall LO, Clarke LP: Review of MR image segmentation techniques using pattern recognition. Med Phys 20:1033-1048, 1993

15. Hall LO, Bensaid AM, Clarke LP, et al: A comparison of neural network and fuzzy clustering techniques in segmenting magnetic resonance images of the brain. IEEE Trans Neural Netw 3:672-682, 1992

16. Kohonen T: Self-organization and associative memory. New York, NY, Springer-Verlag, 1984

17. Cannon RL, Dave JB, Bezdek JC: Efficient implementation of the fuzzy c-mean clustering algorithms. IEEE Trans on Pattern Analysis and Machine Intelligence 8:248-255, 1996

18. Bezdek JC, Tsao EC, Pal NR: Fuzzy Kohonen clustering networks. Proc IEEE Intl Conf Fuzzy Systems, San Diego, CA, 1992, pp 1035-1043

19. Chuang KH, Chiu MJ, Lin CC, et al: Model-free functional MRI analysis using Kohonen clustering neural network and fuzzy c-means. IEEE Trans Med Imaging 18:1117-1128, 1999

20. Chiu MJ: Image analysis and application on neuroscience of fMRI. Doctoral Dissertation. Taipei, National Taiwan University, 2000

21. Bottomley PA, Foster TH, Argersinger RE, et al: A review of normal tissue hydrogen NMR relaxation times and relaxation mechanisms from 1-100 MHz: Dependence on tissue type, NMR frequency, temperature, excision and age. Med Physics 11:425-448, 1984

22. Bottomley PA, Hardy CF, Argersinger RE, et al: A review of ^{1}H nuclear magnetic resonance relaxation in pathology: Are T1 and T2 diagnostic? Med Physics 14:1-37, 1987

23. Posin JP, Ortendahl DA, Hylton NM, et al: Variable magnetic resonance imaging parameters: Effect on detection and characterization of lesions. Radiology 155:719-725, 1985

24. Kim SG, Tsekos NV: Perfusion imaging by a flow-sensitive alternating inversion recovery (Fair) technique: Application to functional brain imaging. Magn Reson Med 37:425-435, 1997

25. McKeown MJ, Makeig S, Brown GG, et al: Analysis of fMRI data by blind separation into independent spatial components. Hum Brain Mapping 6:160-188, 1998